Vibro-acoustic response of flexible Micro-Perforated Plates: impact of the boundary condition at the perforation walls

J. Tournadre [1], **M. A. Temiz** [2], **P. Martínez-Lera** [3], **W. De Roeck** [1], **W. Desmet** [1,4]
[1] KU Leuven, Department of Mechanical Engineering,
Celestijnenlaan 300 B, 3001, Heverlee, Belgium
e-mail: **jonathan.tournadre@kuleuven.be**

[2] Eindhoven University of Technology, Department of Mechanical Engineering,
PO Box 513, 5600 MB, Eindhoven, The Netherlands

[3] Siemens Industry Software,
Researchpark 1237, Interleuvenlaan 87, 3001, Leuven, Belgium

[4] Member of Flanders Make

Abstract

This paper investigates the vibro-acoustic behavior of flexible micro-perforated plates through a finite element method approach, in which each single orifice can be modeled independently. The role of the vibrations on the local orifice impedance values is included in the numerical model and analyzed for the case of PVC perforated plates with different orifice sizes. Two expressions for the modified local orifice impedance are compared, depending on the extension of the correction to the attached mass of air at the orifice ends or not. The effect on the global plate absorption properties is quantified. It is found that accounting for the orifice impedance alteration through the structural motion is more important for larger orifice diameters and at low frequency. This effect is nevertheless rather limited for the investigated micro-perforated plates and can be neglected in first instance.

Preprint

1 Introduction

Micro-perforated plates (MPPs) have been a popular subject in acoustics since their high potential in sound absorption was pointed out by Maa [1]. Mounted on top of a cavity, they benefit from an increased absorption bandwidth compared to purely reactive sound absorbers, due to the viscous dissipation taking place at the small perforations. MPPs have the extra advantage that they can be produced from a large number of materials, broadening their range of applications from room acoustic panels to industrial applications like automotive mufflers. Depending on the plate material and dimensions, the effects of vibrations on the acoustic response of a MPP can be of major importance. As the plate porosity decreases, the effect of plate vibration tends to increase [2]. It is therefore to be considered when studying MPPs or flexible MMPs (f-MPPs) as sound absorbers, as typical open area ratios are of the order of $1\,\%$. This issue should be addressed in the early stages of the design process. The role of vibrations on the acoustic characterization of MMPs has been first noticed by Lee and Swenson, as an additional absorption peak [3].

A standard way to investigate the vibro-acoustic behavior of micro-perforated panels is the fully coupled modal approach, in which both structural motion of the perforated panel and the acoustic field are described in terms of their constituting modes. Such a theoretical model requires the a priori knowledge of the modal decomposition of the structural response of the perforated plate. It is therefore limited to cases with simple

geometrical configurations. On the other hand, it delivers a set of equations which is fast to solve and provides an efficient tool for optimization purposes. Such a modal approach has been applied, through the years, to the study of both Helmholtz-type and panel-type resonances, from the case of an infinite plate backed by a cavity [4] to cases of finite perforated plates and membranes [5, 6], and multi-layer micro-perforated absorbers [7].

In a previous work [8], a numerical Finite Element Method (FEM) model based on the representation of each single orifice has been investigated as an alternative to the modal approach. It consists of solving in a direct manner the set of equation resulting from the coupled vibro-acoustic problem. This approach has shown to deliver results with good agreements compared to experimental data from the literature [9]. The presented FEM model offers an additional flexibility in terms of design estimation for f-MPP, as no structural modes are imposed, allowing the use of more complex geometry and boundary conditions for the plate structure. It gives as well a handy investigation tools for the overall positioning of the orifices for design optimization.

In all the previously mentioned works, the acoustic impedance of the orifices has been assumed homogeneous through the entire plate and determined from the standard Maa model under rigid-wall assumption [1]. The effect of the vibrations on the orifice impedance itself is therefore entirely neglected. The aim of this work is to investigate, for the case of micro-perforated plates, the impact of the structural vibrations on the acoustic impedance of the orifices constituting the perforated plate. For this purpose, the alternative boundary condition at the inner orifice walls proposed by Li [10], which was applied and verified in the case of perforated membranes, will be investigated for the case of a MPP placed inside an impedance tube (see Fig. 1). This is done in the present FEM model through an additional step in which the modified local orifice impedance is determined from the previously computed plate impedance. The coupled vibro-acoustic system is then solved using the local acoustic impedance values for each orifice. The global impact of this additional step in the numerical modeling of a circular f-MPP will be quantified for different orifice diameters in terms of the absorption coefficient of the complete MPP. The particular question to know if this impedance correction should be extended or not to the air mass attached at the orifice ends will be further discussed with some quantitative arguments.

Preprint

The paper is organized as follows. In Sec. 2, the expressions for the local orifice impedance accounting for the plate vibration are presented, along with the theoretical treatment of the plate motion. Sec. 3.1 describes the coupled vibro-acoustic problem and the numerical FEM model for its resolution. The investigated configuration of a MPP inside an impedance tube is detailed in Sec. 3.2. Finally, the results on the computed plate impedances, on the modified orifice impedance values and on the overall acoustic responses of the perforated plates are shown and discussed in Sec. 4.

2 Modified impedance model accounting for the local displacement of the plate

2.1 Modified orifice transfer impedance

In most of the studies on the vibro-acoustic response of micro-perforated plates/panels in the literature, the impedance chosen to describe the acoustic behavior of the perforations is based on Maa's classical model. This model is derived assuming a rigid plate [11], for which $v_{\text{plate}} = 0$. The fluid particle velocity at the hole wall $v(r = r_p)$ is taken equal to zero (see Fig. 2), and the effect of the plate vibration on the acoustic impedance of the perforations is neglected. Under these assumptions, the normalized acoustic transfer impedance for a single perforation z_p is given by $z_{p,\text{Maa}}$ [1]:

$$z_{p,\text{Maa}} = \frac{\Delta p}{\bar{v}\rho_0 c_0} = \underbrace{\frac{j\omega t_p}{c_0}\left[1 - \frac{2}{Sh\sqrt{-j}}\frac{J_1(Sh\sqrt{-j})}{J_0(Sh\sqrt{-j})}\right]^{-1}}_{z_{p,\text{Maa-inner}}} + \underbrace{\frac{2}{c_0\rho_0}\alpha R_s + j\delta\omega\frac{r_p}{c_0}}_{z_{p,\text{Maa-outer}}}, \tag{1}$$

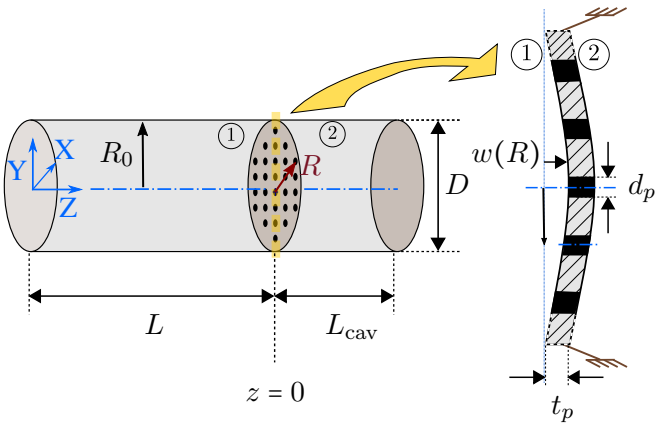

Figure 1: Configuration for the circular MPP clamped inside an impedance tube.

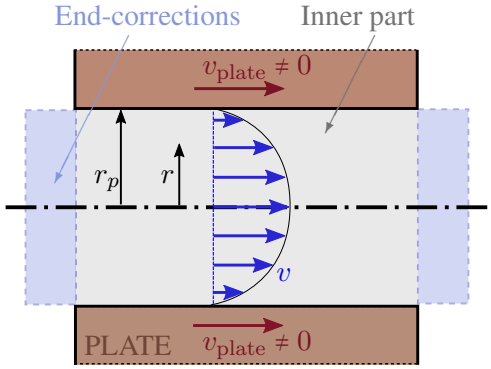

Figure 2: Description of the velocity field $v(r)$ in the local coordinate system for each single perforation.

where $\Delta p = p_1 - p_2$ is the sound pressure difference between the two ends of the orifice tube, $\bar{v}$ is the averaged acoustic particle velocity in the perforation, t_p is the orifice length (equal to the plate thickness), J_n is the Bessel function of the first kind of order n, $Sh = d_p\sqrt{\omega\rho_0/(4\mu)}$ is the Shear number with μ and ρ_0 the dynamic viscosity and the density of the acoustic medium (i.e. air in this study), respectively. c_0 is the speed of sound in the medium. The term $z_{p,\text{Maa-inner}}$ represents only the inertial and damping effects happening inside the orifice length. The contribution of the end-corrections $z_{p,\text{Maa-outer}}$ to the total normalized orifice impedance $z_{p,\text{Maa}}$ is defined by the surface resistance $R_s = 0.5\sqrt{2\mu\rho_0\omega}$, and both resistive and reactive end-correction coefficients α and δ (see [12]).

Preprint

Li *et al.* [10], in a work on the acoustic behavior of perforated membranes, proposed recently an alternative to the classical Maa's model by modifying the boundary condition at the wall inside a perforation to account for a non-zero plate velocity. The fluid particles adhere at the moving hole wall boundary due to the no-slip boundary condition, and therefore their velocity is supposed to be equal to the panel/membrane velocity. The proposed velocity boundary condition, expressed as a function of the distance r from the perforation axis in the local coordinate of an orifice of radius r_p, is expressed as

$$v(r = r_p) = v_{\text{plate}} \neq 0\,. \tag{2}$$

Applying the boundary condition (2) to the general solution of the motion equation of the fluid particles inside a cylindrical (axisymmetric) orifice [13], short compared to the acoustic wavelength, leads to the following expression for the particle velocity inside a hole:

$$v(r) = v_{\text{plate}}\frac{J_0(k_\text{a} r)}{J_0(k_\text{a} r_p)} - \frac{\Delta p}{t_p \mu k_\text{a}^2}\left[1 - \frac{J_0(k_\text{a} r)}{J_0(k_\text{a} r_p)}\right], \tag{3}$$

where $k_\text{a}^2 = -j\rho_0\omega/\mu = -j(Sh/r_p)^2$, with Sh the Shear number.

The expression (3) can be integrated over the area of the orifice section to compute an averaged particle velocity $\bar{v}$, and the following formula can be derived [10] for the normalized acoustic impedance of a single hole:

$$z_p = \frac{\Delta p}{\bar{v}\rho_0 c_0} = \frac{1}{\rho_0 c_0 \dfrac{v_{\text{plate}}}{\Delta p}\dfrac{2}{k_\text{a} r_p}\dfrac{J_1(k_\text{a} r_p)}{J_0(k_\text{a} r_p)} + \dfrac{c_0}{j\omega t_p}\left[1 - \dfrac{2}{k_\text{a} r_p}\dfrac{J_1(k_\text{a} r_p)}{J_0(k_\text{a} r_p)}\right]}\,. \tag{4}$$

The second term of the denominator in Eq. (4) corresponds to the internal part of the hole acoustic impedance under Maa's rigid wall assumption $z_{p,\text{Maa-inner}}$.

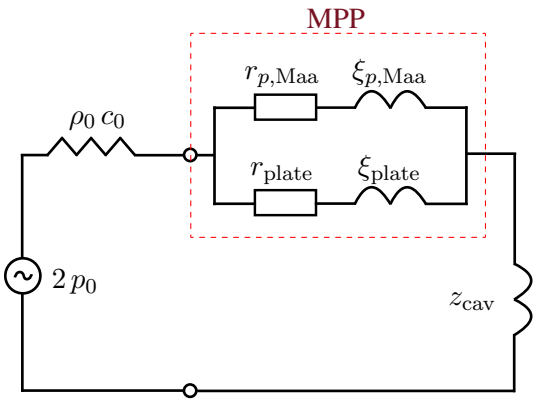

(a) Standard representation of the complete system constituted of the MPP and the backing cavity - case with no effect of the plate vibrations on the impedance of the orifices: $z \equiv$ impedance, $r \equiv$ resistance, and $\xi \equiv$ reactance.

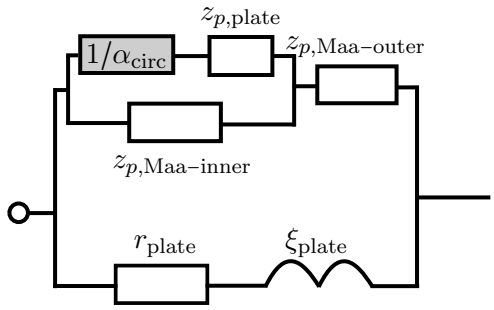

(b) Case with only impact of the vibrations on the inner part of the orifice impedance.

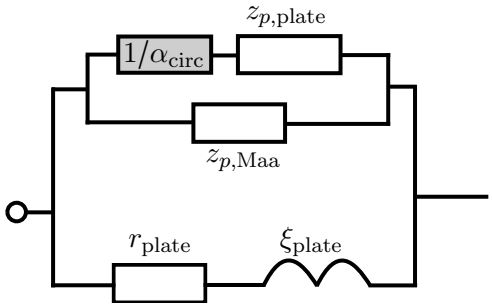

(c) Case with the correction due to plate vibrations applied to the complete orifice impedance.

Figure 3: Electrical analogy for the investigated system.

Preprint

The term $z_{\mathrm{plate}} = \Delta p/(\rho_0 c_0 v_{\mathrm{plate}})$ in Eq. (4) can be defined as the local normalized impedance of the plate. Equation (4) describes the direct effect of the plate vibration on the local orifice acoustic impedance. This correction of the orifice impedance at a position R from the center of the plate is thus given by

$$z_p(R) = \frac{1}{\dfrac{\alpha_{\mathrm{circ}}}{z_{\mathrm{plate}}(R)} + \dfrac{1}{z_{p,\mathrm{Maa-inner}}}}, \tag{5}$$

where

$$\alpha_{\mathrm{circ}} = \frac{2}{Sh\sqrt{-j}} \frac{J_1(Sh\sqrt{-j})}{J_0(Sh\sqrt{-j})} \tag{6}$$

is a weighting factor linked to the orifice circular shape, and depending only on the Shear number Sh for the given circular geometry. As it is highlighted in Eq. (5), the analytical expression of the correction to be applied on the orifice acoustic impedance is derived only for the internal part, and neglects the effect of vibration on the end-corrections. No evidence has yet been shown that this correction can be applied similarly to the resistive and reactive contributions related to the attached mass of air outside of the orifice. The precise answer to this question is beyond the scope of the present paper and cannot be treated with the numerical model used here. It is nevertheless possible to assess in the present study the relevance of this consideration for the acoustic behavior of the vibrating MPP. For this purpose, the two following limit cases will be investigated: applying the correction to only the internal part of the orifice impedance and keeping the end-corrections unaltered by the vibration (7a), and applying the correction to the complete orifice impedance (7b). Equation (7b) corresponds to the case where the plate vibration is considered affecting in a similar manner both the orifice inner part and the attached mass of air on the sides, whereas Eq. (7a) disregards entirely the effect of the vibration on the outer air mass. The final expressions used for the acoustic

impedance of one perforation at the location R are thus the following:

$$z_p(R) = \begin{cases} z_p(R) = \dfrac{1}{\dfrac{\alpha_{\text{circ}}}{z_{\text{plate}}(R)} + \dfrac{1}{z_{p,\text{Maa-inner}}}} + z_{p,\text{Maa-outer}}\,, & \text{(7a)} \\ z_p(R) = \dfrac{1}{\dfrac{\alpha_{\text{circ}}}{z_{\text{plate}}(R)} + \dfrac{1}{z_{p,\text{Maa}}}} & \text{(7b)} \end{cases}$$

In [10], the expression (7b) is applied. We will quantify in this work the differences between the previous two assumptions for the case of f-MPPs, both in terms of local acoustic impedance and global acoustic response. Figure 3 illustrates, through an electrical analogy, the different modeling options compared in this study for a MPP. As the plate impedance is a complex number, the vibration can be expected to affect both resistive and reactive parts of the orifice impedance (see Eq. (5)). This point will be discussed further in Sec. 4.

2.2 Vibration of thin plate

In order to compute the local value of the orifice impedance accounting for the plate vibration, it is shown necessary, from Eq. (7), to know the value of the plate impedance z_{plate} at the orifice position. The present work is limited to the case of a circular plate placed in a duct (see Fig. 1). For such a simple geometry, an analytical treatment of the structural behavior of the plate is often applied in the literature [9]. This theoretical approach is briefly described here and will be further compared to the obtained MPP behavior gotten from Finite Element Method treatment.

Preprint

The flexible MPP is assumed to behave as a thin, homogeneous plate of radius $R_0 = D/2$. This means that the hole diameters and the open surface ratios are considered sufficiently small that the effect of the perforations on the plate motion can be neglected. Therefore the structural analysis will be limited here to the symmetric vibrations of a uniform circular diaphragm, with the local displacement $w(R)$ of the plate only depending on the radial position R from the plate center (see Fig. 1). The equation of motion for the thin plate, whose restoring force results from its stiffness, is given by [14]:

$$D_p \nabla^4 w(R) - \rho_p t_p \omega^2 w(R) = \Delta p\,, \tag{8}$$

where ρ_p is the volume density of the material, Δp is the external pressure difference acting as driving force on the plate surface; $D_p = E(1+j\eta)t_p^3/[12(1-\nu^2)]$ is the flexural rigidity where E is the Young's modulus, η is the loss factor, $j = \sqrt{-1}$ is the imaginary number and ν is the Poisson ratio of the MPP material. Applied oscillatory forces are assumed. The steady-state solution for the local plate displacement $w(R)$ has thus the form $w(R) = \Psi(R)e^{j\omega t}$. For this particular circular symmetry case, and by further assuming perfectly clamped condition at the boundary in contact with the duct wall, i.e. $\Psi(R_0) = 0$ and $\partial\Psi/\partial r(R_0) = 0$, the complete solution of Eq. (8) is given by

$$\Psi(R) = \frac{\Delta p}{\rho_p t_p \omega^2}\left[\frac{J_0(\frac{\gamma_m}{R_0}R) - \frac{J_1(\gamma_m)}{I_1(\gamma_m)}I_0(\frac{\gamma_m}{R_0}R)}{J_0(\gamma_m) - \frac{J_1(\gamma_m)}{I_1(\gamma_m)}I_0(\gamma_m)} - 1\right], \tag{9}$$

with J_j and I_j are the jth order Bessel functions and modified Bessel functions of the first kind. For a given m^{th} modal vibration, the parameter γ_m, which is a constant for the present clamped condition, is defined by the following transcendental equation

$$\frac{J_0(\gamma_m)}{J_1(\gamma_m)} = -\frac{I_0(\gamma_m)}{I_1(\gamma_m)}\,. \tag{10}$$

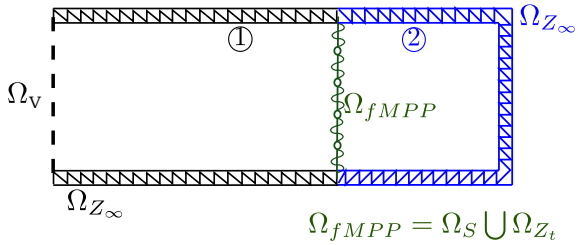

Figure 4: Schematic representation of the coupled vibro-acoustic numerical model for the configuration of a f-MPP inside an impedance tube.

From the value of γ_m given by Eq. (10), the natural frequencies of the clamped thin plate can be computed by

$$f_{n,m} = \frac{t_p \gamma_m^2}{2\pi R_0^2} \sqrt{\left(\frac{E(1+j\eta)}{12\rho_p(1-\nu^2)} \right)}. \tag{11}$$

In the present frequency domain Finite Element Method framework, the displacements of the plate are numerically computed from a first coupled vibro-acoustic simulation, where an homogeneous orifice impedance is imposed for all orifices over the plate. From this step, the MPP velocity field $v_{\text{plate}}(R)$ is derived from the computed displacement $w(R)$. The pressure fields on both sides of the MPP are further extracted to obtain the averaged pressure difference Δp through the plate. This allows to compute the local values of the plate impedance

$$z_{\text{plate}}(R) = \frac{\Delta p}{v_{\text{plate}}(R)}. \tag{12}$$

Preprint

The corrected impedance value for an orifice at the position R can be obtained using Eq. (7). The fully coupled vibro-acoustic problem is finally run again with, this time, the locally modified orifice impedance values.

3 Numerical model and study case

3.1 Finite Element Model for the coupled vibro-acoustic system

The numerical model is built in 3-D within LMS Virtual.Lab® [15]. The discretized problem is solved through a FEM formulation in the frequency domain. The schematic description of the configuration is illustrated in Fig. 4. Assuming harmonic plane waves and neglecting the thermal and viscous effects in the acoustic mediums ① and ② shown in Fig. 1, the acoustic wave equation in frequency domain is given by the Helmholtz equation

$$\omega^2 p_n(z) + c_0^2 \nabla^2 p_n(z) = 0, \tag{13}$$

where $\omega = 2\pi f$ is the radial frequency, c_0 is the speed of sound, ∇^2 is the *Laplacian* operator, and p_n is the acoustic pressure in medium ⓝ. The acoustic domains ① and ② are governed by this equation. High-order Lobatto shape functions are used to described the discrete field of pressure. The inlet Ω_V is defined by an imposed velocity boundary V_{in}, with a chosen velocity amplitude $|V_{in}| = 1\,\text{m/s}$ here.

Due to the small thickness of the MPPs considered, it is appropriate to assume that the displacement field $w(R)$ can be characterized in terms of the displacement components of the shell middle surface. The thin MPP is therefore modeled as a combination of 2-D elastic shell elements to solve for the plate structural displacement field, and of imposed transfer impedance boundary Ω_{Z_t} to model the acoustic behavior of each

perforation. The vibro-acoustic coupling boundary Ω_S, between the surfaces of the acoustic domain and the structural shell elements, is defined by the following relations:

$$F = p_1(Z = 0^-) - p_2(Z = 0^+)\,, \tag{14a}$$

$$v_{1,2}(R, 0) = j\omega w(R)\,, \tag{14b}$$

where F is the point force acting on the plate surface and v is the velocity. Equation (14b) ensures the continuity of the normal shell velocities and the normal fluid velocities at the fluid-structure coupling interface. The remaining boundaries are defined as hard-wall boundary, Ω_{Z_∞}.

The resulting finite element model for the unconstrained degrees of freedom of the coupled vibro-acoustic problem takes the form:

$$\left\{\begin{bmatrix}\mathbf{K}_s & \mathbf{K}_c\\ 0 & \mathbf{K}_a\end{bmatrix} + j\omega\begin{bmatrix}\mathbf{C}_s & 0\\ 0 & \mathbf{C}_a\end{bmatrix} - \omega^2\begin{bmatrix}\mathbf{M}_s & 0\\ \mathbf{M}_c & \mathbf{M}_a\end{bmatrix}\right\}\begin{Bmatrix}\mathbf{w}_u\\ \mathbf{p}_u\end{Bmatrix} = \begin{Bmatrix}\mathbf{F}_{si}\\ \mathbf{F}_{ai}\end{Bmatrix}, \tag{15}$$

where $\mathbf{K}$ is the stiffness, $\mathbf{M}$ is the mass, $\mathbf{C}$ is the dissipation and $\mathbf{F}$ is the forcing matrix. The subscripts 'a', 's' and 'c' represent the words *acoustic*, *structural* and *coupling*. The vectors $\mathbf{w}_u$ and $\mathbf{p}_u$ represent the degrees of freedom for the plate displacement and acoustic pressure vectors that need to be solved for. The stiffness coupling matrix $\mathbf{K}_c$ represents the force loading of the fluid on the structure, which is proportional to the pressure. The coupled mass matrix $\mathbf{M}_c$ expresses the structural force applied on the fluid, which is proportional to the plate acceleration. The forcing matrices $\mathbf{F}_{ai}$ and $\mathbf{F}_{si}$ introduce the prescribed pressure and displacement vectors into the set of equations.

The described FEM approach for investigating the problem of f-MPP has already been successfully compared to measurement and literature data for validation [8]. The present work aims at introducing the additional impact of the plate vibration on the local orifice acoustic impedance, following the methodology detailed in Sec. 2.2. The influence of accounting or not for this phenomenon is evaluated for the global acoustic absorption characteristic of the investigated f-MPP geometries. It is done by calculating the absorption coefficient $\beta = 1 - |p^-/p^+|^2$, where p^+ and p^- are the complex amplitudes of the left and right traveling pressure waves in domain ① and can be calculated by using the standard multi-microphone method [16] in the plane wave regime. The frequency range of this work, defined by $f \in [125\,\mathrm{Hz} - 2000\,\mathrm{Hz}]$, satisfies this assumption for the chosen dimensions of the impedance tube.

Preprint

3.2 Study case of a circular MPP in an impedance tube

The configuration in this work is represented in Fig. 1, and consists of a perforated plate of diameter $D = 100\,\mathrm{mm}$ and thickness $t_p = 0.5\,\mathrm{mm}$. To study the effect of the modified boundary condition applied to the orifice impedance, different orifice sizes are considered. The plates are constituted from 69 perforations of diameters $d_p = 0.5\,\mathrm{mm}$ for the case $\mathcal{P}1$, $d_p = 1\,\mathrm{mm}$ for the case $\mathcal{P}2$, and $d_p = 2\,\mathrm{mm}$ for the case $\mathcal{P}3$. The configuration of a plate without perforation (referred as the case $\mathcal{NP}$) is included in this work as well, for the analysis of the impact of perforation size on the modified plate impedance. The structural parameters such as the Young's modulus E, Poisson ratio ν and the loss factor η of the MPP are listed, along with the geometrical parameters, in the Table 1.

The modified orifice impedance, as defined in Eq. (7), is spatially varying over the plate, depending on the position of the orifice considered. The FEM representation allows to define the exact acoustic impedance for each of the orifices. Nevertheless, for practical reason in the present axisymmetric configuration, orifices have been grouped by zones, as illustrated in Fig. 5, depending on their distance to the plate center. An averaged impedance value is assigned for all the orifices inside one specific zone. In the presented case, the plate area is divided into five zones with respective orifice impedance $Z_{p,i}$, for $i \in \{1, .., 5\}$.

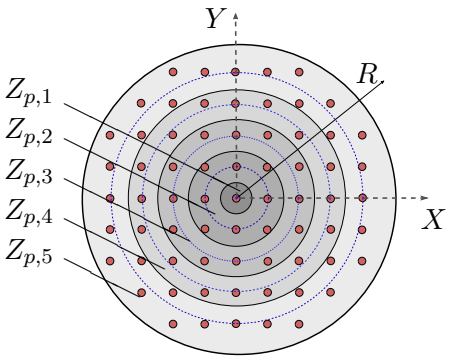

Figure 5: Zonal splitting of the plate surface to defined the local values for the orifice impedance, depending on the distance R from the plate center: orifice surface area, impedance zones, (- - -) position chosen for impedance estimation.

Parameter	**Case** $\mathcal{NP}$	**Case** $\mathcal{P}1$	**Case** $\mathcal{P}2$	**Case** $\mathcal{P}3$
d_p [mm]	N/A	0.50	1	2.0
t_p [mm]	0.50			
b [mm]	N/A	10	10	10
n_p [-]	69			
σ [-]	0 %	0.2 %	0.7 %	2.8 %
D [mm]	100			
L [mm]	300			
L_{cav} [mm]	50			
E [N/m^2]	3×10^9			
η [-]	0.03			
ν [-]	0.3			

Table 1: Configuration parameters of the study cases.

4 Results and discussions

4.1 Vibro-acoustic response of the MPP and plate impedance

Preprint

To start this results section, a closer look is taken on the plate displacement field $\Psi(R)$. Figure 6 shows the absolute value of the numerically computed plate displacement $|\Psi_{num}|$ at frequencies close to the first three natural frequencies of the plate $f_{n,1/2/3}$. The displacement fields found match with the shapes of the normal axi-symmetric modes for a plate with fixed rim, as expressed in Eq. (9). The modes (0,1), (0,2) and (0,3) are shown for the case $d_p = 2\,\text{mm}$ in Fig. 6a, Fig. 6b and Fig. 6c, respectively. Figure 6d presents the obtained plate absorption coefficient over the frequency range $f \in [125\,\text{Hz} - 2000\,\text{Hz}]$, for both perforations of diameter $d_p = 0.5\,\text{mm}$ (—♦—) and $2\,\text{mm}$ (—o—). For both curves, the absorption peaks related to the Helmholtz-type resonance (around $400\,\text{Hz}$ and $850\,\text{Hz}$, respectively), and the two peaks linked to panel-type resonance (the ones closer to the plate natural frequencies) can be clearly observed. No peak can be observed near the first natural frequency $f_{n,1}$. This is due to the stronger coupling between the first plate structural mode and the Helmholtz resonance. The latter phenomenon is driving this peak frequency. For the case with $d_p = 0.5\,\text{mm}$, the panel-type resonance peaks visible in the absorption curve of Fig. 6d are very close to the analytically estimated natural frequencies of the plate. For the larger orifice diameter case, those peaks are shifted towards lower frequency values. It can result from the effect of the increased porosity on the structural behavior of the plate (explained by a decreased stiffness compared to the $\mathcal{NP}$ case) or from the vibro-acoustic coupling itself. The higher the order of the plate mode, the less coupling happens with the

	Plate structural mode i	1	2	3	4
Ⓐ	Analytical natural frequency $f_{n,i}$ [Hz]	149.5	582	1304	2315
Ⓑ	Computed resonance frequency $f_{n,i}^{\text{num}}$ [Hz]	272	590	1291	
Ⓒ	Computed structural peak frequency $f_{\text{peak},i}^{\text{num}}$ for $d_p = 0.5\,\text{mm}$ [Hz]	-	595	1288	
Ⓓ	Computed structural peak frequency $f_{\text{peak},i}^{\text{num}}$ for $d_p = 2\,\text{mm}$ [Hz]	-	561	1271	

Table 2: Summary of the peak frequencies obtained for the vibro-acoustic response of the investigated plates.

Helmholtz-type resonance. It appears that mostly the two first plate vibration modes are relevant for the vibro-acoustic coupling in the present MPP configuration. Looking at the Helmholtz-type resonance peak frequencies obtained from the coupled vibro-acoustic problem compared to the ones by neglecting the plate motion, it shows also that the vibro-coupling is stronger for orifices of small dimensions.

Table 2 summarizes the peak frequencies obtained from: Ⓐ the plate natural frequencies from the analytical expression defined by Eq. (11) assuming no effect of the perforations on the structural modes, Ⓑ the resonance peak frequencies computed with the present FEM approach for a non-perforated plate (see [8]), Ⓒ with perforation diameter $d_p = 0.5\,\mathrm{mm}$ and Ⓓ with perforation diameter $d_p = 2\,\mathrm{mm}$.

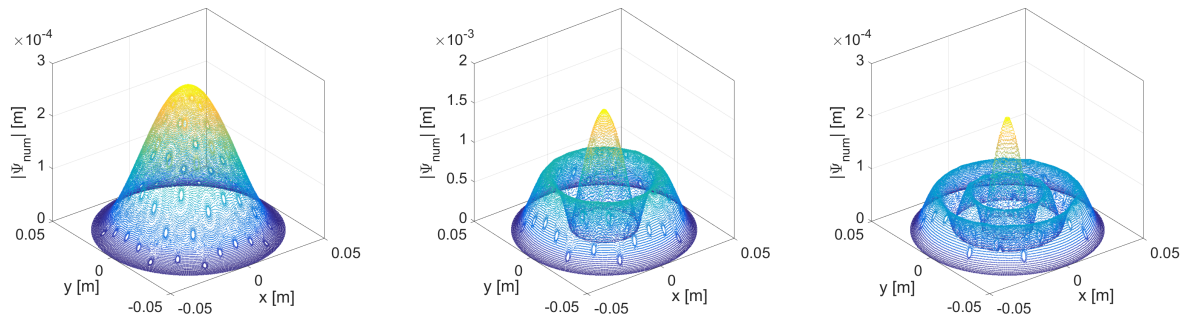

(a) Ψ_{num} at 150 Hz (b) Ψ_{num} at 575 Hz (c) Ψ_{num} at 1300 Hz

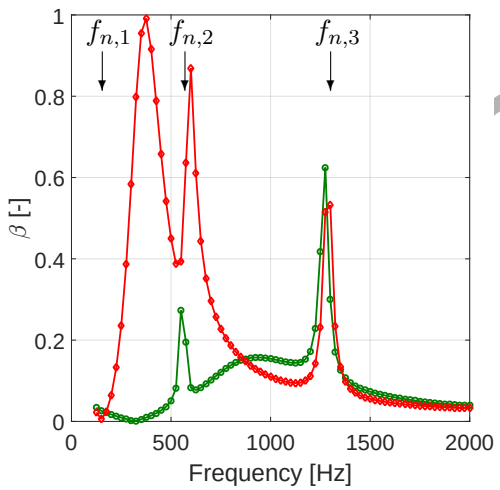

(d) Absorption coefficient β

Figure 6: Magnitude of the plate displacement field obtained numerically $|\Psi_{num}|$ for the frequencies $f = 150\,\mathrm{Hz}$ (a), $f = 575\,\mathrm{Hz}$ (b), and $f = 1300\,\mathrm{Hz}$ (c) for the case $\mathcal{P}3$ (i.e. $d = 2\,\mathrm{mm}$). (d) Absorption coefficient β in function of the frequency from the direct fully coupled vibro-acoustic FEM solver: (—◇—) $d_p = 0.5\,\mathrm{mm}$ and (—○—) $d_p = 2\,\mathrm{mm}$.

To judge the impact of the additional perforations on the structural behavior of the circular plate itself, the computed plate impedance $z_{\mathrm{plate}}(R)$ for the different perforation sizes is compared and confronted to the no-perforation case. The values of the plate impedance at the center of the plate $z_{\mathrm{plate}}(0)$ are shown in Fig. 7, as well as the absolute changes compared to the no-perforation reference case. It appears that the effect on the plate impedance due to the presence of perforations is very limited. The impedance curves divert further from the reference case as the orifice size increases, but nevertheless the impact is kept small for the investigated cases, as the porosity values are also small (max. 2.7 %). The absolute changes in terms of impedance appear predominant in-between the natural frequencies (see Fig. 7c). Due to this little impact of the perforations on the structural response of the plate, the analytical expression of the plate impedance (derived from Eq. (9)

by using $v(R) = j\omega\Psi(R)$) can be used to correct the local orifice impedance z_p. Nevertheless, the plate impedance used in this work is the one directly computed from the coupled vibro-acoustic FEM solver.

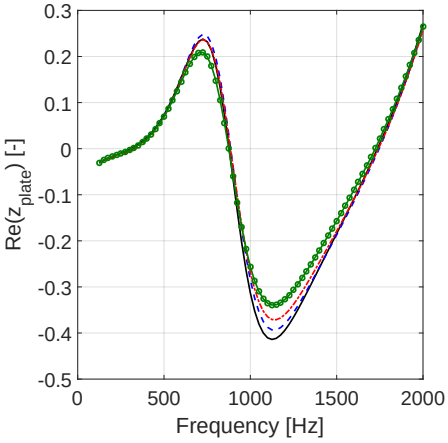

(a) Normalized plate resistance

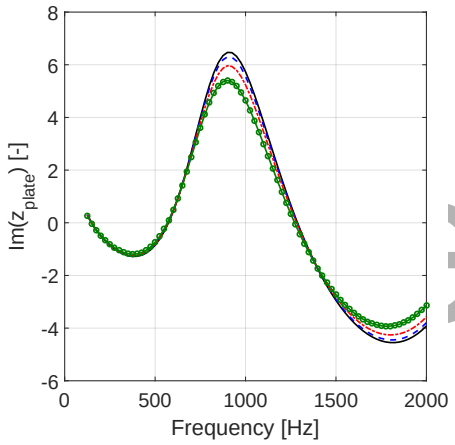

(b) Normalized plate reactance

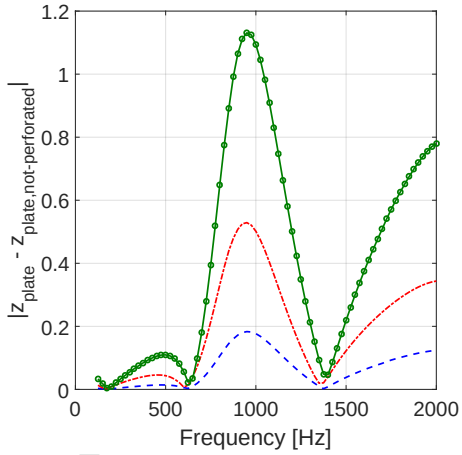

(c) Absolute change in plate impedance z_{plate} compared to the case without perforation $\mathcal{NP}$.

eprint

Figure 7: Impact of the orifices on the normalized plate impedance z_{plate} at the center of the duct (R=0): case with no perforation (——) and cases with orifices of diameter $d = 0.5\,\text{mm}$ (- - -), $d = 1\,\text{mm}$ (-·-·-), and $d = 2\,\text{mm}$ (-o-).

4.2 Impact on single orifice impedance

This section presents the corrected orifice impedance accounting for the local velocity of the MPP, as given by the two expressions of Eq. (7a) and Eq. (7b). Results are shown here for a single orifice, at a given location R from the plate center.

Figure 8 illustrates, for two orifice geometries, the corrected orifice impedance computed from Eq. (7b) at different locations on the plate. The correction accounting for the plate impedance influences the orifice impedance predominantly near the plate natural frequencies. Over the remaining of the frequency range, the impedance is very close to the value obtained under rigid-wall assumption. Unlike the results for membranes presented in [10], the impact on the orifice reactance is observed to be negligible (see Fig. 8a and Fig. 8b) for the considered perforated plates. The impedance correction mostly impacts the resistive part. The modification appears to be of the same magnitude for both orifice sizes (mainly because the plate impedance. i.e. the correction, is independent of the orifice size), but as the resistance is higher for the smallest dimension, the relative change is lower for small orifices. It is therefore expected to get more impact of the investigated

effect for large orifices than smaller ones, as will be shown for the absorption coefficient β in Sec. 4.3. Comparing the values at different radial locations on the plate, the closer to the center the orifice is, the more effective are the vibrations on its local impedance. This is consistent with the clamped condition applied on the rim of the plate, limiting the plate motion closeby. As expected, the impedance values computed at $R = 0.05\,\mathrm{m}$, i.e. on the plate edge, gives a similar result as the standard impedance model neglecting vibration effects, as $\Psi(R = 0.05) = 0$ is imposed.

Figure 9 compares the impedance values obtained from the two proposed corrections (see Eq. (7)) for an orifice placed at the center of the plate. The same trend for the corrected impedance is observed from both corrections. Including the end-correction part to the correction (—+— curve) as defined by Eq. (7b) delivers however significantly more deviation from the standard impedance values (—— curve).

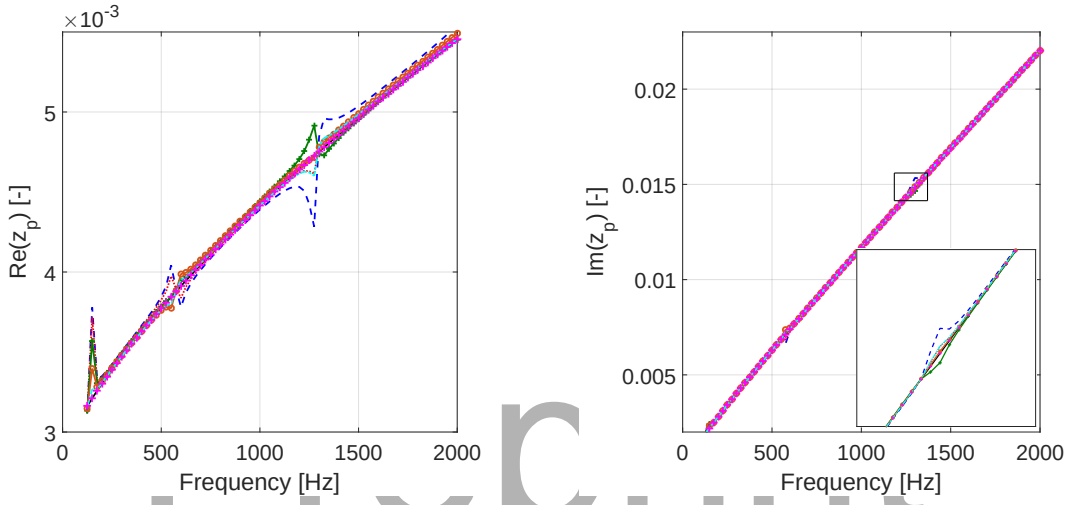

(a) Orifice diameter $d_p = 0.5\,\mathrm{mm}$

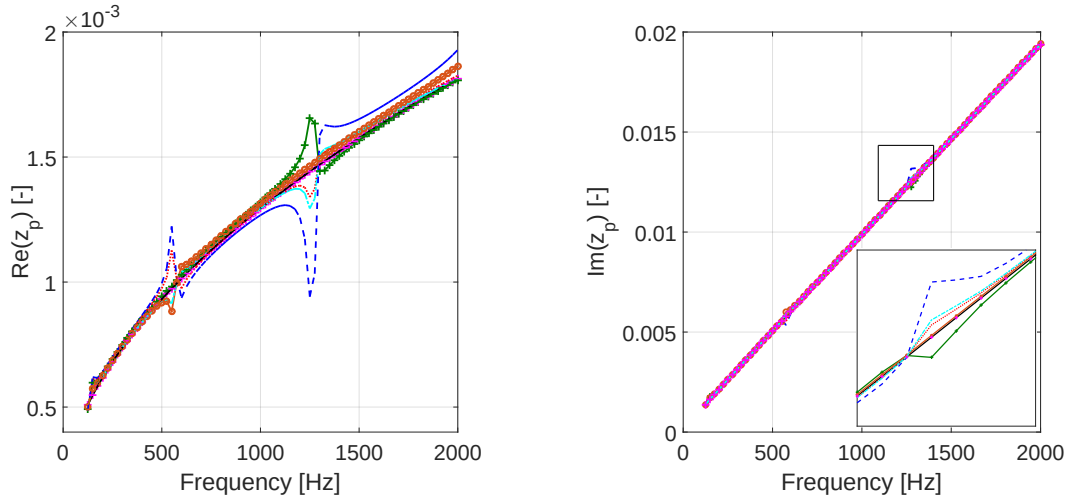

(b) Orifice diameter $d_p = 2\,\mathrm{mm}$

Figure 8: Normalized resistance $\mathrm{Re}(z_p)$ (left) and reactance $\mathrm{Im}(z_p)$ (right) of a single orifice, depending on its location: homogeneous Maa impedance (——) compared to the corrected impedance of an orifice at $R = 0\,\mathrm{m}$ (- - -), $R = 0.01\,\mathrm{m}$ (·····), $R = 0.02\,\mathrm{m}$ (—+—), $R = 0.03\,\mathrm{m}$ (—o—), $R = 0.04\,\mathrm{m}$ (-·-·-), and $R = 0.05\,\mathrm{m}$ (+).

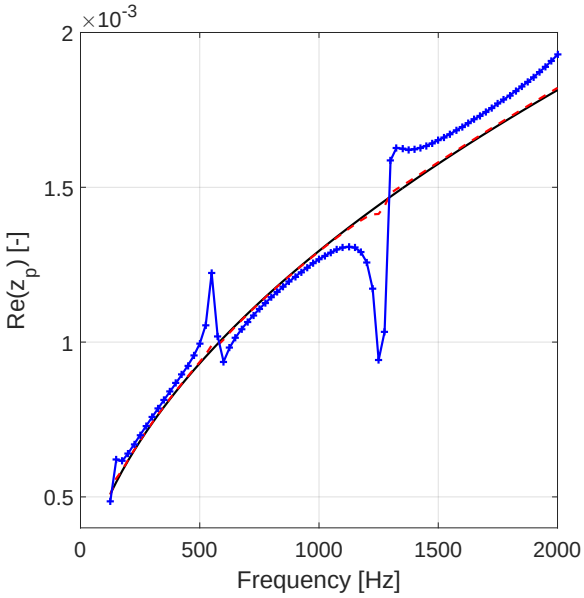

Figure 9: Modified normalized resistance Re(z_p) for an orifice of d_p = 2 mm at the center of the plate (R = 0): (- - -) correction applied to the inner part only as defined in Eq. (7a), (—+—) extended to the end-corrections terms as defined in Eq. (7b), and (——) reference Maa model.

Preprint

4.3 Global effect on MPP absorption coefficient

After having observed the local changes in impedance which ensue from the modified boundary condition at the inner wall of the orifices, the global impact on the acoustic behavior of the MPP is analyzed and quantified in the following. Results are presented here in terms of MPP absorption coefficient β. These absorption curves have been obtained from the numerically computed pressure fields by standard multi-microphone approach from different probes placed inside the duct domain, as mentioned in Sec. 3.1. The absorption coefficient obtained from orifice impedance under Maa's rigid wall assumption (β) will be compared to the corrected ones (β^*), resulting from the modified boundary condition at the orifice wall. Results with both corrections, defined by Eq. (7), are presented.

Figure 10 shows, for two different sizes of orifice (d_p = 0.5 mm in Fig. 10a and d_p = 2 mm in Fig. 10b), the relative changes in terms of absorption coefficient. The impact on the absorption curve by accounting for the vibration effect on the orifice impedance is overall of limited magnitude for the investigated cases. It is only of significance for the low frequency range, and predominantly near the first MPP natural frequency. For the rest of the spectrum, the changes are kept below 1 %. Note that the 2nd peak in Fig. 10b, appearing at 325 Hz, is not relevant because the absorption coefficient itself is very close to zero. This does not appear for the case with d_p = 0.5 mm. We only get one peak in relative change of β^* which matches with a natural frequency, i.e. the 1st one. Considering the absolute changes (not represented here), the impedance modification has an impact 4 times larger on the absorption coefficient for d_p = 2 mm than for d_p = 0.5 mm. Another appearing trend is that the absorption coefficient is not modified the most, in relative consideration, at the natural frequency but left and right near this natural frequency. It is important to remember that the correction on the orifice impedance is only affecting the numerical model on the surface related to the orifices. Therefore, the impact of the modified boundary condition at the orifice inner wall is weighted by the porosity of the plate. As the porosities of the investigated plate samples are rather low (max. 2.8 %), the influence on the MPP absorption curve is limited.

The effect of vibration on the orifice impedance appears to be more important for the case with the largest

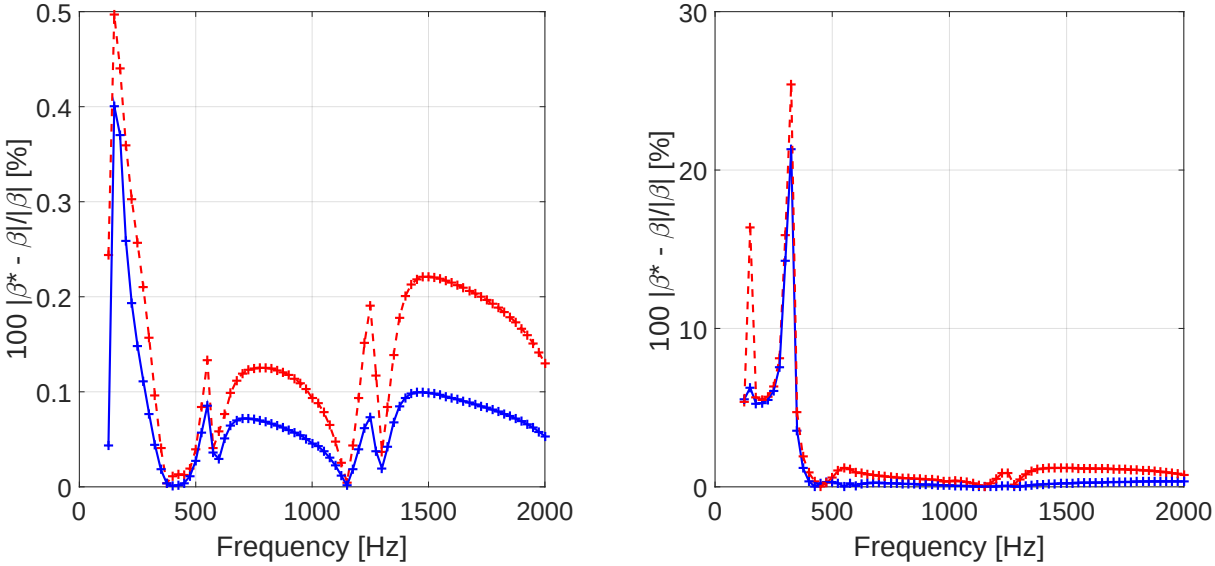

(a) Case of orifices with a diameter $d_p = 0.5\,\mathrm{mm}$

(b) Case of orifices with a diameter $d_p = 2\,\mathrm{mm}$

Figure 10: Relative change in the MPP absorption coefficient β^* due to the modified orifice impedance, compared to absorption coefficient obtained with the standard Maa Model case β: impedance correction done on the complete impedance (- +-), correction on the internal part only (—+—).

Preprint

orifice diameter. This can stem from two facts. First, the relative change in resistance due to the vibration is found larger for large orifices, because the resistance is overall lower. Secondly, the increase in orifice size leads, in the present case of a fixed number of perforations in the plate, to larger porosity values. This larger porosity delivers more weight to the modified orifice impedance.

Applying the correction to the complete orifice impedance leads, as expected from the local impedance curves, e.g. Fig. 9, to larger relative changes in terms of absorption coefficient. The trends between the curves are very similar, but extending the correction to the end-correction part of the Maa impedance model appears to strengthen considerably its effect, over the entire frequency range. Following what has been stated before, this is again mostly of importance for the low frequency and the lowest plate natural frequency.

5 Conclusions

This paper explores the impact of the vibrations on the orifice acoustic impedance and the consequences for the absorption performance of MPPs. The numerical vibro-acoustic FEM model, in which each orifice can be modeled independently, allows to define a local value for the impedance of each orifice depending on the plate impedance. Unlike the case of membranes, vibrations are found to only alter the resistive part of the orifice impedance. Due to the role of the plate impedance for the modified orifice acoustic impedance, a detailed analysis of the plate displacements in presence of the orifices has been done. For the investigated MPPs, only the two first structural modes seem to participate to the vibro-acoustic coupling. The presence of the orifices has shown to have a small impact on the obtained plate impedance but could be still responsible for a shift in panel-type resonance peak frequencies.

Two expressions for the modified local orifice impedance have been compared. Including the effect of vibrations on the end-corrections appears to be as important as the contribution of the orifice inner part. Applying the correction to the sum of the impedance related to the attached air mass at the orifice ends and the internal part is nevertheless not justified by the theory and results are presented here as a limit case to

show the implications linked to this particular phenomenon. An exact answer would require to solve the coupled vibro-acoustic problem for a moving orifice considering the viscous-thermal losses.

The results for the absorption curves of MPPs with different orifice size have shown that accounting for the orifice impedance alteration through the structural motion is more important for larger orifice diameters and at low frequency. This effect is nevertheless rather limited for the investigated micro-perforated plates. It is however expected to be more significant for perforates with a higher porosity. For the present configurations, this effect can be neglected without it leading to significant error on the absorption characteristics of the MPPs.

Acknowledgements

Authors gratefully acknowledge the financial support from the Research Fund KU Leuven, as well as from the European Commission provided in the framework of the FP7 Marie Curie Initial Training Network TANGO (GA 316654) and of the FP7 Collaborative Project IDEALVENT (GA 314066).

References

[1] D.-Y. Maa, *Potential of microperforated panel absorber*, Journal of the Acoustical Society of America, Vol. 104, No. 5, (1998), pp. 2861–2866.

[2] D. Takahashi, M. Tanaka, *Flexural vibration of perforated plates and porous elastic materials under acoustic loading*, Journal of the Acoustical Society of America, Vol. 112, No. 4, (2002), pp. 1456–1464.

[3] J. Lee, G. W. Swenson, *Cavity sound absorbers for low frequencies*, Noise Control Engineering Journal, Vol. 38, No. 3, (1992), pp. 109–117.

[4] K. Sakagami, D. Takahashi, H. Gen, M. Morimoto, *Acoustic properties of an infinite elastic plate with a back cavity*, Acta Acustica United with Acustica, Vol. 78, No. 5, (1993), pp. 288–295.

[5] Y. Y. Lee, E. W. M. Lee, C. Ng, *Sound absorption of a finite flexible micro-perforated panel backed by an air cavity*, Journal of Sound and Vibration, Vol. 287, No. 1-2, (2005), pp. 227–243.

[6] T. Bravo, C. Maury, C. Pinhéde, *Sound absorption and transmission through flexible micro-perforated panels backed by an air layer and thin plate*, Journal of the Acoustical Society of America, Vol. 131, No. 5, (2012), pp. 3853–3863.

[7] T. Bravo, C. Maury, D. Pinhède, *Enhancing sound absorption and transmission through flexible multi-layer micro-perforated structures*, Journal of the Acoustical Society of America, Vol. 134, No. 5, (2013), pp. 3663–3673.

[8] M. Temiz, J. Tournadre, I. Lopez Arteaga, P. Martínez-Lera, A. Hirschberg, *Numerical estimation of the absorption coefficient of flexible micro-perforated plates in an impedance tube*, *Proceedings of The 23rd International Congress on Sound and Vibration, Athens, Greece, 2016 10-14 July*, Athens (2016).

[9] M. Toyoda, R. L. Mu, D. Takahashi, *Relationship between Helmholtz-resonance absorption and panel-type absorption in finite flexible microperforated-panel absorbers*, Journal of Applied Acoustics, Vol. 71, No. 4, (2010), pp. 315–320.

[10] C. Li, B. Cazzolato, A. Zander, *Acoustic impedance of micro perforated membranes: velocity continuity condition at the perforation boundary*, Journal of the Acoustical Society of America, Vol. 139, No. 1, (2016), pp. 93–103.

Preprint

[11] D.-Y. Maa, *Theory and design of microperforated-panel sound-absorbing construction*, Science China Mathematics, Vol. 18, No. 1, (1975), pp. 55–71.

[12] M. A. Temiz, I. Lopez-Artega, G. Efraimsson, M. Åbom, A. Hirschberg, *The influence of edge geometry on end-correction coefficient in micro perforated plates*, Journal of the Acoustical Society of America, Vol. 138, No. 6, (2015), pp. 3668–3677.

[13] I. B. Crandall, *Theory of vibrating systems and sound*, D. Van Nostrand Company (1926).

[14] G. Kirchhoff, *Über das Gleichgewicht und die Bewegung einer elastischen Scheibe*, Journal für die reine und angewandte Mathematik, Vol. 40, (1850), pp. 51–88.

[15] *Siemens PLM Software, LMS Virtual.Lab 13.5* (2015), https://www.plm.automation.siemens.com.

[16] M. Åbom, *Measurement of the scattering matrix of acoustical two-ports*, Journal of Mechanical Systems and Signal Processing, Vol. 5, No. 2, (1991), pp. 89–104.

Preprint